

Stability of general relativistic Miyamoto-Nagai galaxies

M. Ujevic,^{1*} and P. S. Letelier²

¹*Centro de Ciências Naturais e Humanas, Universidade Federal do ABC, 09210-170, Santo André, São Paulo, Brasil*

²*Departamento de Matemática Aplicada, Instituto de Matemática, Estatística e Computação Científica
Universidade Estadual de Campinas, 13081-970, Campinas, São Paulo, Brasil*

ABSTRACT

The stability of a recently proposed general relativistic model of galaxies is studied in some detail. This model is a general relativistic version of the well known Miyamoto-Nagai model that represents well a thick galactic disk. The stability of the disk is investigated under a general first order perturbation keeping the spacetime metric frozen (no gravitational radiation is taken into account). We find that the stability is associated with the thickness of the disk. We have that flat galaxies have more not-stable modes than the thick ones i.e., flat galaxies have a tendency to form more complex structures like rings, bars and spiral arms.

Key words: relativity – galaxies: kinematics and dynamics

1 INTRODUCTION

The natural shape of an isolated self-gravitating fluid is axially symmetric. For this reason, exact axial symmetric solutions of Einstein field equations are good candidates to model astrophysical bodies in General Relativity. In the last decades, several exact solutions were studied as possible galactic models. Static thin disk solutions were first studied by Bonnor & Sackfield (1968) and Morgan & Morgan (1969), where they considered disks without radial pressure. Disks with radial pressure and with radial tension had been considered by Morgan & Morgan (1970) and González & Letelier (1999), respectively. Self-similar static disks were studied by Lynden-Bell & Pineault (1978), and Lemos (1989). Moreover, solutions that involve superpositions of black holes with static disks were analyzed by Lemos & Letelier (1993, 1994, 1996) and Klein (1997). Also, relativistic counter-rotating thin disks as sources of the Kerr type metrics were found by Bičák & Ledvinka (1993). Counter-rotating models with radial pressure and dust disks without radial pressure were studied by González & Espitia (2003), and García & González (2004), respectively; while rotating disks with heat flow were studied by González & Letelier (2000). Furthermore, static thin disks as sources of known vacuum spacetimes from the Chazy-Curzon metric (Chazy 1924; Curzon 1924) and Zipoy-Voorhees (Zipoy 1966; Voorhees 1970) metric were obtained by Bičák, Lynden-Bell & Katz (1993). Also, Bičák, Lynden-Bell & Pichon (1993) found an

infinite number of new relativistic static solutions that correspond to the classical galactic disk potentials of Kuzmin & Toomre (Kuzmin 1956; Toomre 1963) and Mestel & Kalnajs (Mestel 1963; Kalnajs 1972). Stationary disk models including electric fields (Ledvinka, Zofka & Bičák 1999), magnetic fields (Letelier 1999), and both electric and magnetic fields (Katz, Bičák & Lynden-Bell 1999) had been studied. In the last years, exact solutions for thin disks made with single and composite halos of matter (Vogt & Letelier 2003), charged dust (Vogt & Letelier 2004a) and charged perfect fluid (Vogt & Letelier 2004b) were obtained. For a survey on relativistic gravitating disks, see Semerák (2002) and Karas, Huré & Semerák (2004). Most of the models constructed above were found using the metric to calculate its energy momentum-tensor, i.e. an inverse problem. Several exact disk solutions were found using the direct method that consists in computing the metric for a given energy momentum tensor representing the disk (Neugebauer & Meinel 1995; Klein & Richter 1999; Klein 2001; Frauendiener & Klein 2001; Klein 2002, 2003a,b). In a first approximation, the galaxies can be thought to be thin, what usually simplifies the analysis and provides very useful information. But, in order to model real physical galaxies the thickness of the disks must be considered. Exact axially symmetric relativistic thick disks in different coordinate systems were studied by González & Letelier (2004). Also, different thick disks were obtained from the Schwarzschild metric in different coordinates systems with the “displace, cut, fill, and reflect” method (Vogt & Letelier 2005a).

The applicability of these disks models to any structure found in Nature lays in its stability. The study of the stability, analytically or numerically, is vital to the acceptance of a particular model. Also, the study of different

* E-mail: mujevic@ufabc.edu.br (MU); letelier@ime.unicamp.br (PSL)

types of perturbations, when applied to these models, might give an insight on the formation of bars, rings or different stellar patterns. Moreover, a perturbation can cause the collapse of a stable object with the posterior appearance of a different kind of structure. An analytical treatment of the stability of disks in Newtonian theory can be found in Binney & Tremaine (1987), Fridman & Polyachenko (1984) and references therein. In general, the stability of disks in General Relativity is done in two ways. One way is to study the stability of the particle orbits along geodesics. This kind of study was made by Letelier (2003) transforming the Rayleigh criterion of stability (Lord Rayleigh 1916; Landau & Lifshitz 1987) into a general relativistic formulation. Using this criterion, the stability of orbits around black holes surrounded by disks, rings and multipolar fields were analyzed (Letelier 2003). Also, this criterion was employed by Vogt & Letelier (2003) to study the stability of the isotropic Schwarzschild thin disk, and thin disks of single and composite halos. The stability of circular orbits in stationary axisymmetric spacetimes was studied by Bardeen (1970) and Abramowicz & Prasanna (1990). Moreover, the stability of circular orbits of the Lemos-Letelier solution (Lemos & Letelier 1994) for the superposition of a black hole and a flat ring was considered by Semerák & Žáček (2000a,b) and Semerák (2003). Also, Bičák, Lynden-Bell & Katz (1993) analyzed the stability of several thin disks without radial pressure or tension studying their velocity curves and specific angular momentum. Another way of studying the stability of disks is perturbing its energy momentum tensor. This way is more complete than the analysis of particle motions along geodesics, because we are taking into account the collective behavior of the particles. However, there are few studies in the literature performing this kind of perturbation. A general stability study of a relativistic fluid, with both bulk and dynamical viscosity, was done by Seguin (1975). He considered the coefficients of the perturbed variables as constants, i.e. local perturbations. Usually, this condition is too restrictive. Stability analysis of thin disks from the Schwarzschild metric, the Chazy-Curzon metric and Zipoy-Voorhees metric, perturbing their energy momentum tensor with a general first order perturbation, were made by Ujevic & Letelier (2004), finding that the thin disks without radial pressure are not stable. Moreover, stability analysis of the static isotropic Schwarzschild thick disk as well as the general perturbation equations for thick disks were studied by Ujevic & Letelier (2007).

In Newtonian gravity, models for globular clusters and spherical galaxies were developed by Plummer (1911) and King (1966). In the case of disk galaxies, important thick disk models were obtained by Miyamoto & Nagai (Miyamoto & Nagai 1975; Nagai & Miyamoto 1976) from the prior work of Kuzmin (1956) and Toomre (1963) about thin disks galaxies. Miyamoto and Nagai “thickened-up” Toomre’s series of disk models and obtained pairs of three-dimensional potential and density functions. Also, Satoh (1980) obtained a family of three-dimensional axisymmetric mass distribution from the higher order Plummer models. The Miyamoto-Nagai potential shares many of the important properties of actual galaxies, especially the contour plots of the mass distribution which are qualitatively similar to the light distribution of disk galaxies (Binney & Tremaine

1987). Recently, two different extensions of the Miyamoto-Nagai potential appeared in the literature: a triaxial generalization (Vogt & Letelier 2007) which has as a particular case the original axially symmetric model, and a relativistic version (Vogt & Letelier 2005b) which has as a Newtonian limit the same original model.

In order to have a general relativistic physical model for galaxies, we must consider, first of all, the thickness of the disk and its stability under perturbations of the fluid quantities. The purpose of this work is to study numerically the stability of the general relativistic Miyamoto-Nagai disk under a general first order perturbation. The perturbation is done in the temporal, radial, axial and azimuthal components of the quantities involved in the energy momentum tensor of the fluid. In the general thick disk case (Ujevic & Letelier 2007), the number of unknowns is larger than the number of equations. This opens the possibility of performing several types of combinations of the perturbed quantities. In this manuscript we search for perturbations in which a perturbation in a given direction of the pressure creates a perturbation in the same direction of the four velocity. The energy momentum perturbation considered in this manuscript is treated as “test matter”, so it does not modified the background metric obtained from the solution of Einstein equations.

The article is organized as follows. In Sec. 2, we present the general perturbed conservation equations for the thick disk case. The energy momentum tensor is considered diagonal with all its elements different from zero. Also, in particular, we discuss the perturbations that will be considered in some detail in the next sections of this work. In Sec. 3, we present the thick disk model whose stability is analyzed, i.e. the general relativistic Miyamoto-Nagai disk. The form of its energy density and pressures, as well as, the restrictions that the thermodynamic quantities must obey to satisfy the strong, weak and dominant energy conditions are shown. Later, in Sec. 4, we perform the perturbations to the general relativistic Miyamoto-Nagai disk; in particular we study its stability. Finally, in Sec. 5, we summarize our results.

2 PERTURBED EQUATIONS

The thick disk considered is a particular case of the general static-axially-symmetric metric

$$ds^2 = -e^{2\Psi_1} dt^2 + e^{2\Psi_2} R^2 d\theta^2 + e^{2\Psi_3} (dR^2 + dz^2), \quad (1)$$

where Ψ_1 , Ψ_2 and Ψ_3 are functions of the variables (R, z) . (Our conventions are: $G = c = 1$, metric signature $+2$, partial and covariant derivatives with respect to the coordinate x^μ denoted by $_{,\mu}$ and $_{;\mu}$, respectively.)

In its rest frame, the energy momentum tensor of the fluid $T^{\mu\nu}$ is diagonal with components $(-\rho, p_R, p_\theta, p_z)$, where ρ is the total energy density and (p_R, p_θ, p_z) are the radial, azimuthal and axial pressures or tensions, respectively. So, in this frame of reference, the energy momentum tensor can be written as

$$T^{\mu\nu} = \rho U^\mu U^\nu + p_R X^\mu X^\nu + p_\theta Y^\mu Y^\nu + p_z Z^\mu Z^\nu, \quad (2)$$

where U^μ , X^μ , Y^μ , and Z^μ are the four vectors of the orthonormal tetrad

$$\begin{aligned}
 U^\mu &= e^{-\Psi_1}(1, 0, 0, 0), \\
 X^\mu &= e^{-\Psi_3}(0, 1, 0, 0), \\
 Y^\mu &= \frac{e^{-\Psi_2}}{R}(0, 0, 1, 0), \\
 Z^\mu &= e^{-\Psi_3}(0, 0, 0, 1),
 \end{aligned} \tag{3}$$

which satisfy the orthonormal relations. Note that with the above definitions, the timelike four velocity of the fluid is U^μ and the quantities X^μ , Y^μ , and Z^μ are the spacelike principal directions of the fluid. Furthermore, the energy momentum tensor satisfies Einstein field equations, $G_{\mu\nu} = 8\pi T_{\mu\nu}$. Moreover, the quantities involved in the energy momentum tensor and the coefficients of the perturbed conservation equations are functions of the coordinates (R, z) only. Let us consider a general perturbation A_P^μ of a quantity A^μ of the form

$$A_P^\mu(t, R, \theta, z) = A^\mu(R, z) + \delta A^\mu(R, z)e^{i(k_\theta\theta - \omega t)} \tag{4}$$

where $A^\mu(R, z)$ is the unperturbed quantity and $\delta A^\mu(R, z)e^{i(k_\theta\theta - \omega t)}$ is the perturbation. Replacing (4) for each quantity in the energy momentum tensor (2) and calculating the perturbed energy momentum equations, $\delta T_{;\nu}^{\mu\nu} = 0$, we obtain

$$\mu = t$$

$$\begin{aligned}
 &\delta U_{,R}^R(\rho U^t + \xi_1 p_R X^R) + \delta U_{,z}^z(\rho U^t + \xi_3 p_z Z^z) \\
 &+ \delta U^R[F(t, R, \rho U^t) + \xi_{1,R} p_R X^R + \xi_1 F(t, R, p_R X^R)] \\
 &+ \delta U^\theta[ik_\theta(\rho U^t + \xi_2 p_\theta Y^\theta)] \\
 &+ \delta U^z[F(t, z, \rho U^t) + \xi_{3,z} p_z Z^z + \xi_3 F(t, z, p_z Z^z)] \\
 &+ \delta \rho(-i\omega U^t U^t) = 0,
 \end{aligned} \tag{5}$$

$$\mu = R$$

$$\begin{aligned}
 &\delta p_{R,R}(X^R X^R) + \delta U^R[-i\omega(\rho U^t + \xi_1 p_R X^R)] \\
 &+ \delta \rho(U^t U^t \Gamma_{tt}^R) + \delta p_R G(R, R, X^R X^R) \\
 &+ \delta p_\theta(Y^\theta Y^\theta \Gamma_{\theta\theta}^R) + \delta p_z(Z^z Z^z \Gamma_{zz}^R) = 0,
 \end{aligned} \tag{6}$$

$$\mu = \theta$$

$$\delta U^\theta[-\omega(\rho U^t + \xi_2 p_\theta Y^\theta)] + \delta p_\theta(k_\theta Y^\theta Y^\theta) = 0, \tag{7}$$

$$\mu = z$$

$$\begin{aligned}
 &\delta p_{z,z}(Z^z Z^z) + \delta U^z[-i\omega(\rho U^t + \xi_3 p_z Z^z)] \\
 &+ \delta \rho(U^t U^t \Gamma_{tt}^z) + \delta p_R(X^R X^R \Gamma_{RR}^z) \\
 &+ \delta p_\theta(Y^\theta Y^\theta \Gamma_{\theta\theta}^z) + \delta p_z G(z, z, Z^z Z^z) = 0.
 \end{aligned} \tag{8}$$

where

$$F(I, J, K) = K_{,J} + K(2\Gamma_{IJ}^I + \Gamma_{\alpha J}^\alpha), \tag{9}$$

$$G(I, J, K) = K_{,J} + K(\Gamma_{IJ}^I + \Gamma_{\alpha J}^\alpha), \tag{10}$$

and $\Gamma_{\beta\gamma}^\alpha$ are the Christoffel symbols. In finding Eqs. (5)-(8) we assumed that the perturbed energy momentum tensor does not modify the background metric. Also, we disregard terms of order greater or equal to δ^2 . For details see Ujevic & Letelier (2004, 2007).

Besides the four equations furnished by the energy momentum conservation equations, $T_{;\nu}^{\mu\nu} = 0$, there is another important conservation equation, the equation of continuity,

$$(nU^\mu)_{;\mu} = 0, \tag{11}$$

where n is the proper number density of particles. The proper number density of particles n , and the total energy density ρ are related through the relation,

$$\rho = nm_b + \varepsilon, \tag{12}$$

where m_b is the constant mean baryon mass and ε the internal energy density. Multiplying Eq. (12) by U^μ , performing the covariant derivative $(; \mu)$ and using Eq. (11), we obtain that

$$(\rho U^\mu)_{;\mu} = (\varepsilon U^\mu)_{;\mu}. \tag{13}$$

Now, from the relation $U_\nu T_{;\mu}^{\mu\nu} = 0$ and the energy momentum tensor (2), we obtain an expression for $(\rho U^\mu)_{;\mu}$. Substituting this last expression into Eq. (13) we finally arrive to

$$(\varepsilon U^\mu)_{;\mu} = p_R X^\mu U_\nu X_{;\mu}^\nu + p_\theta Y^\mu U_\nu Y_{;\mu}^\nu + p_z Z^\mu U_\nu Z_{;\mu}^\nu, \tag{14}$$

which is a first order differential equation for ε . Therefore, with ε given by (14) the equation of continuity (11) is satisfied. For this reason, the continuity equation can be omitted in our stability analysis because, in principle, we can always find a solution for ε . Hereafter, the contribution of nm_b and ε to the total energy density are taken into account in ρ . In the case in which the internal energy density of the fluid is given, the equation of continuity must be considered. The thermodynamic properties of the system can be obtained from observations or theoretically, e.g. from the Fokker-Planck equation, where we obtain the particle distribution function of the disk. Solving the three dimensional Fokker-Planck equation is not an easy task, but some progress in Newtonian gravity had been done (Ujevic & Letelier 2005, 2006).

The four equations, (5)-(8), contain seven independent unknowns, say $\delta U^R, \delta U^\theta, \delta U^z, \delta \rho, \delta p_R, \delta p_\theta, \delta p_z$. So, at this point, the number of unknowns are greater than the number of equations. This opens the possibility to perform different kind of perturbations. In this article we are interested in perturbations in which the velocity perturbation in a certain direction leads to a pressure perturbation in the same direction. For example, if we perturbed the axial component of the velocity, δU^z , then we must perturb δp_z . With the above criterion, and without imposing any extra conditions to the individual perturbations, only four perturbations combinations are allowed and will be considered in our thick disk model. Furthermore, we perform the perturbation $\delta U^R, \delta p_R, \delta U^z, \delta p_z$ with the extra imposed condition $\delta p_R \equiv \delta p_z$. In this particular case, the system of equations reduces to a second order partial differential equation.

3 GENERAL RELATIVISTIC MIYAMOTO-NAGAI GALAXIES

A static general relativistic version of the Miyamoto-Nagai disk was constructed by Vogt & Letelier (2005b) by making a correspondence between the general isotropic line element in cylindrical coordinates and the Miyamoto-Nagai model (Miyamoto & Nagai 1975; Binney & Tremaine 1987). These general relativistic disks are obtained with (1) and the specializations,

$$\Psi_1 = \ln \left(\frac{1-f}{1+f} \right), \tag{15}$$

$$\Psi_2 = \Psi_3 = 2 \ln(1 + f), \quad (16)$$

where $f = \frac{m}{2\sqrt{R^2 + (a + \sqrt{z^2 + b^2})^2}}$, m is the mass of the disk, and (a, b) are constants that control the shape of the density curves. With this metric, the energy density and pressures for the general relativistic Miyamoto-Nagai disk are

$$\rho = \frac{b^2 [aR^2 + (a + \xi)^2(a + 3\xi)]}{4\pi\xi^3[\frac{1}{2} + \chi]^5}, \quad (17)$$

$$p_R = p_\theta = \frac{b^2 [aR^2 + (a + \xi)^2(a + 2\xi)]}{16\pi\xi^3[\frac{1}{2} + \chi]^5[-\frac{1}{2} + \chi]}, \quad (18)$$

$$p_z = \frac{b^2(a + \xi)^2}{8\pi\xi^2[\frac{1}{2} + \chi]^5[-\frac{1}{2} + \chi]}, \quad (19)$$

where $\xi = \sqrt{z^2 + b^2}$ and $\chi = \sqrt{R^2 + (a + \xi)^2}$. Without losing generality we set $m = 1$ in Eqs. (17)-(19). To satisfy the strong energy condition (gravitational attractive matter) we must have that the “effective Newtonian density” $\Lambda = \rho + p_R + p_\theta + p_z \geq 0$. The weak energy condition requires $\rho \geq 0$ and the dominant energy condition requires $|p_R/\rho| \leq 1$, $|p_\theta/\rho| \leq 1$ and $|p_z/\rho| \leq 1$. The parameters used in this article satisfy all energy conditions. Furthermore, the level curves show that it is physically acceptable. We remark that these are not the only parameters in which the level curves are physically acceptable. In the next section we apply the selected perturbations of Sec. 2 to the general relativistic Miyamoto-Nagai disk mentioned above and study its stability.

4 PERTURBATIONS

Before applying the different kinds of perturbations to the general relativistic Miyamoto-Nagai disk we must do some considerations. Note that the general relativistic Miyamoto-Nagai disk is infinite in the radial and axial directions. We want to study the stability of a finite disk. So, in order to achieve this requirement we need a cutoff in the radial coordinate. In Eqs. (17), (18) and (19), we see that the thermodynamic quantities decrease rapidly enough to define a cutoff in both coordinates. The radial cutoff R_{cut} and the axial cutoff Z_{cut} are set by the following criterion: the energy density within the disk formed by the cutoff parameters has to be more than 90% of the infinite thick disk energy density. The above criterion, and the parameters used in the article, leads to a radial cutoff of $R_{cut} = 10$ units and an axial cutoff of $|Z_{cut}| = 5$ units. The other 10% of the energy density that is distributed from outside the cutoff parameters to infinity can be treated, if necessary, as a perturbation in the outermost boundary condition.

4.1 Perturbation with δU^θ , δp_θ , δU^R , δp_R

We start perturbing the four velocity in its components θ and R . From the physical considerations mentioned in Sec. 2 we also expect variations in the thermodynamic quantities p_θ and p_R . The set of equations (5)-(8) reduces to a second order ordinary differential equation for the perturbation δp_R , say

$$F_A \delta p_{R,RR} + F_B \delta p_{R,R} + F_C \delta p_R = 0, \quad (20)$$

where (F_A, F_B, F_C) are functions of (R, z, w, k_θ) , see Appendix A. For this particular case we have, $\delta p_\theta = -\delta p_R$.

Note that in Eq. (20) the coordinate z only enters as a parameter. Moreover, the equation for δp_R is independent of the parameter w , but w needs to be different from zero to reach that form. The second order equation (20) is solved numerically with two boundary conditions, one at $R \approx 0$ and the other at the radial cutoff. At $R \approx 0$ we set the perturbation δp_R to be $\approx 10\%$ of the unperturbed pressure p_R (18). In the outer radius of the disk we set $\delta p_R|_{R=R_{cut}} = 0$ because we want our perturbation to vanish when approaching the edge of the disk and, in that way, to be in accordance with the applied linear perturbation. We say that our perturbations are valid if their values are lower, or of the same order of magnitude, than the 10% values of its unperturbed quantities.

In Fig. 1, we present the amplitude profile of the radial pressure perturbation in the plane $z = 0$ for different values of the parameters a and b . As in the Newtonian case, the less the ratio b/a , the flatter is the mass distribution. We see that the perturbation δp_R for $(a = 1, b = 1)$ decreases rapidly with R and has oscillatory behavior. At first sight, the perturbation δp_R appears to be stable for all R , but in order to make a complete analysis we have to compare at each radius the values of the perturbations with the values of the radial pressure. For this purpose, we included in the same graph a profile of the 10% value of p_R . We see that the perturbations of δp_R for different values of k_θ are always lower or, at least, of the same order of magnitude when compared to these 10% values. In the flatter case $(a = 1, b = 0.5)$, the perturbation δp_R shows the same qualitative behavior, but the amplitudes of the oscillations are slightly higher. In both cases the amplitudes are well below the 10% values of p_R . If we consider a very flat galaxy $(a = 1, b = 0.1)$ with $w = 1$ we found that some modes are not stable in a small region near the center of the disk, from $R \approx 0$ to $R \approx 0.3$, because the perturbation amplitude is bigger than the 10% value of p_R and our general linear perturbation is no longer valid.

We also performed stability analyses for the physical radial velocity perturbation $\delta \tilde{U}^R = \sqrt{g_{RR}} \delta U^R$ and the physical azimuthal velocity perturbation $\delta \tilde{U}^\theta = \sqrt{g_{\theta\theta}} \delta U^\theta$. Note that our four velocity U^μ (3) has only components in the temporal part, so we do not have values of U^R and U^θ to make comparisons with the perturbed values $\delta \tilde{U}^R$ and $\delta \tilde{U}^\theta$. For that reason we compared, in first approximation, the amplitude profiles of these perturbations with the value of the escape velocity in the Newtonian limit. In the Newtonian limit of General Relativity, $f \ll 1$, we have the well known relation $g_{00} = \eta_{00} + 2\Phi$. So, the Newtonian escape velocity $V_{esc} = \sqrt{2|\Phi|}$ can be written as $V_{esc} = 2\sqrt{f}$, see Vogt & Letelier (2005b). With this criterion, the perturbations $\delta \tilde{U}^r$ and $\delta \tilde{U}^\theta$ are stable because their values are always well below the escape velocity value. Recall that the perturbation δp_R does not depend on the parameter w , but the perturbations $\delta \tilde{U}^R$ and $\delta \tilde{U}^\theta$ do. We performed numerical solutions for the perturbations $\delta \tilde{U}^R$ and $\delta \tilde{U}^\theta$ with different values of the frequency w , and we find that when we increase the value of w the perturbations become more stable.

In this subsection we set the value of the parameter $z = 0$. We performed the same analysis for different values of the parameter $-5 < z < 5$, and we found that the

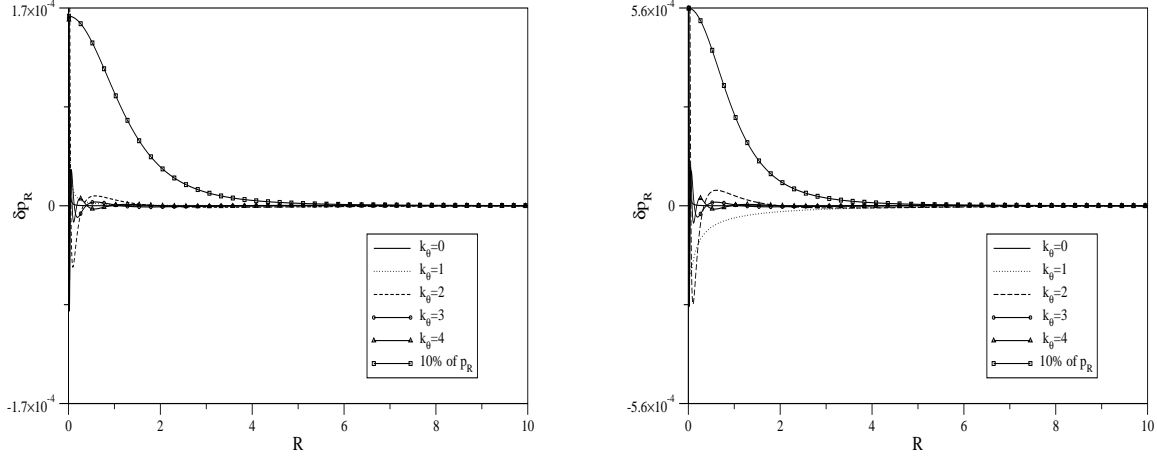


Figure 1. Profiles of the amplitude perturbation for the radial pressure of the fluid for the cases when $z = 0$, $w = 1$ and $k_\theta = 0, 1, 2, 3, 4$. The graph at the left and right correspond to the cases when $(a = 1, b = 1)$ and $(a = 1, b = 0.5)$ respectively. The 10% p_R profile is depicted for better stability comparisons. The modes of these examples are all stable.

perturbations show the same qualitative behavior. Therefore, we can say that the general relativistic Miyamoto-Nagai disk shows some not-stable modes for very flat galaxies, e.g. $(a = 1, b = 0.1)$. Otherwise the disk is stable under perturbations of the form presented in this subsection.

Nevertheless, if we treat the 10% of the energy density as a perturbation in the outermost radius of the disk by setting $\delta p_R|_{R=R_{cut}} = \epsilon$, where $\epsilon < 10\%$ of $p_R|_{R=R_{cut}}$, the qualitative behavior of the mode profiles is the same. In the case of flat galaxies, when they present not stable modes, more complex structures like rings, bars or halos can be formed. Moreover, if we set the frequency $w \rightarrow iw$ we obtain the same equation for the perturbation δp_R , say (20). In this case, the real part of the general perturbation diverges with time and the perturbation is not stable. These last considerations can be applied to every perturbation in the following subsections.

4.2 Perturbation with δU^θ , δp_θ , δU^z , δp_z

In this subsection we perturb the four velocity in its components θ and z , and we expect variations in the thermodynamic quantities p_θ and p_z . The set of equations (5)-(8) reduces to a second order ordinary differential equation for the perturbation δp_z given by

$$F_A \delta p_{z,zz} + F_B \delta p_{z,z} + F_C \delta p_z = 0, \quad (21)$$

where (F_A, F_B, F_C) are functions of (R, z, w, k_θ) , see Appendix B. Note that in Eq. (21) the coordinate R only enters as a parameter. Like the previous case, Eq. (21) is independent of the parameter w , but in order to reach that form we must have w different from zero. The second order equation (21) is solved numerically with two boundary conditions, one in $z = 0$ and the other in $z = Z_{cut}$. At $z = 0$ we set the perturbation δp_z to be $\approx 10\%$ of the unperturbed pressure p_z (19). In the outer plane of the disk we set $\delta p_z|_{z=Z_{cut}} = 0$ because we want our perturbation to vanish when approach-

ing the edge of the disk, and in that way, to be in accordance with the linear perturbation applied.

In Fig 2, we present the amplitude profiles of the axial pressure perturbation, the physical axial velocity perturbation $\delta \tilde{U}^z = \sqrt{g_{zz}} \delta U^z$ and the physical azimuthal velocity perturbation for $R = 0.1$ and different values of the parameters a and b . For comparison reasons, we included in the graphs the amplitude profile that corresponds to 10% of the value of p_z and the escape velocity profile. Note that for $(a = 1, b = 1)$ some modes of the axial pressure perturbation are above the 10% profile of p_z , e.g. the modes with $k_\theta = 0$ and $k_\theta = 5$. In these cases we can say that the mode with $k_\theta = 0$ is not stable and that the mode with $k_\theta = 5$ is near the validity criterion used for the perturbations. These modes are also present in the flatter galaxy $(a = 1, b = 0.5)$ and have the same behaviors. The mode $k_\theta = 5$ is actually not stable. This can be seen in the azimuthal velocity perturbation profiles, where its amplitude is greater than the escape velocity. Note that in the velocity perturbation graphs the mode $k_\theta = 0$ is also not stable. The azimuthal pressure perturbation, not depicted in Fig 2, has all the modes well below the 10% profile of p_θ , and therefore is stable.

The perturbations δp_z and δp_θ do not depend on the parameter w , but the perturbations $\delta \tilde{U}^z$ and $\delta \tilde{U}^\theta$ do. We performed numerical solutions for the perturbations $\delta \tilde{U}^z$ and $\delta \tilde{U}^\theta$ with different values of the frequency w , and we find that when we increase the value of w the perturbations become more stable.

We have performed the same above analysis for different values of the parameter $0 < R < 10$, and we found that the qualitative behavior is the same. We see from Fig. 2 that the not stable modes are more pronounced for the flatter galaxy. Furthermore, for very flat galaxies some modes like $k_\theta = 10$ become not stable. In general, for not stable modes, more complex structures like rings, bars or spiral arms may be formed.

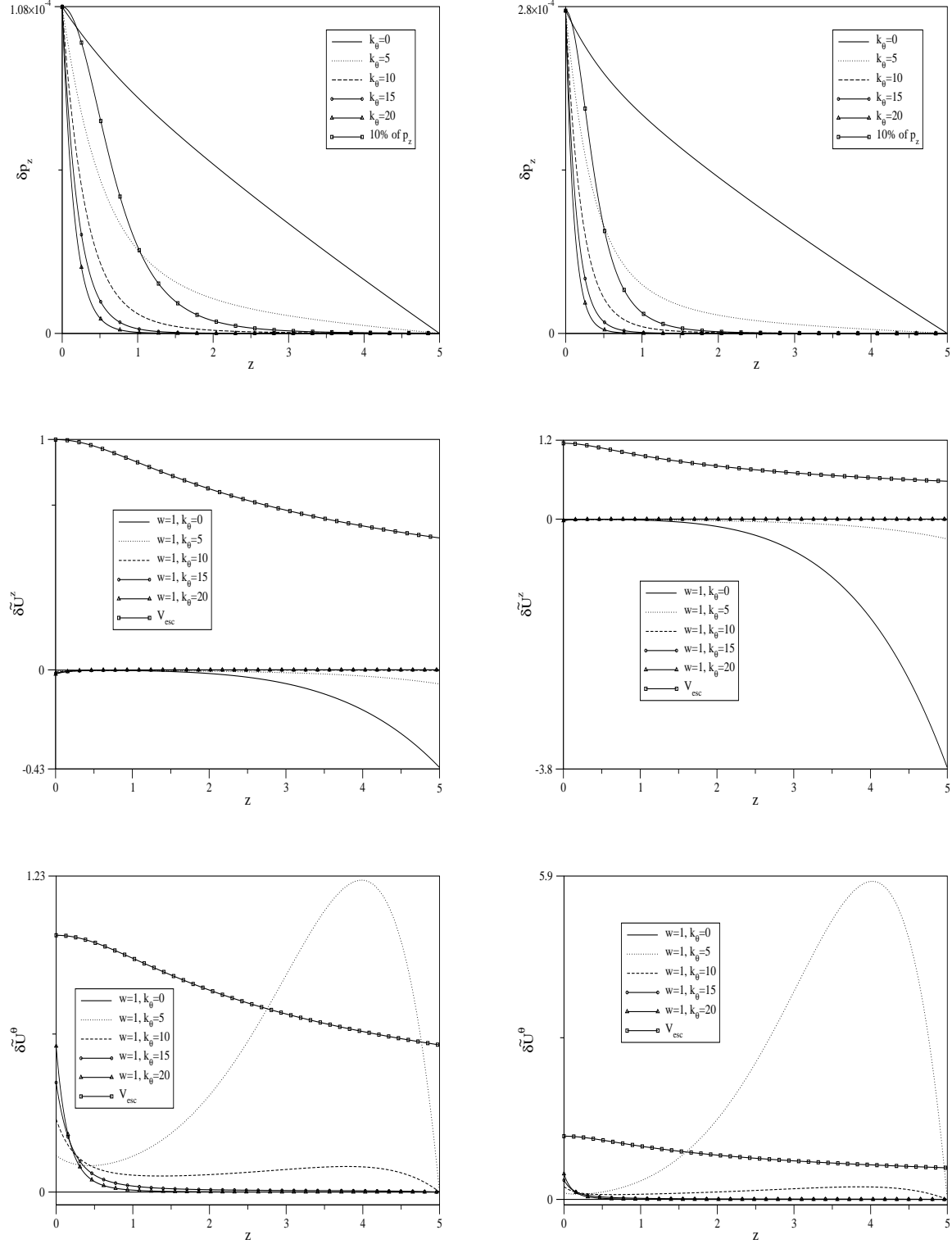


Figure 2. Profiles of the amplitude perturbation for the axial pressure, axial physical velocity and azimuthal physical velocity of the fluid for the cases when $R = 0.1$, and $k_\theta = 0, 5, 10, 15, 20$. The graphs at the left and right correspond to the cases when $(a = 1, b = 1)$ and $(a = 1, b = 0.5)$ respectively. The 10% p_z profile and the escape velocity are depicted for better stability comparisons. Note, in the axial pressure perturbation graph, that some nodes are not stable because they do not satisfy our stability criterion. In order to be stable, a mode must have the correct behavior in all the perturbed quantities. For example, in the case $(a=1, b=1)$ the mode with $w = 1$ and $k_\theta = 5$ seems to be stable in δp_z , but looking into the δU^θ perturbation graph we note that this statement is not true. In the flatter galaxies the modes are not stable on larger regions of the domain.

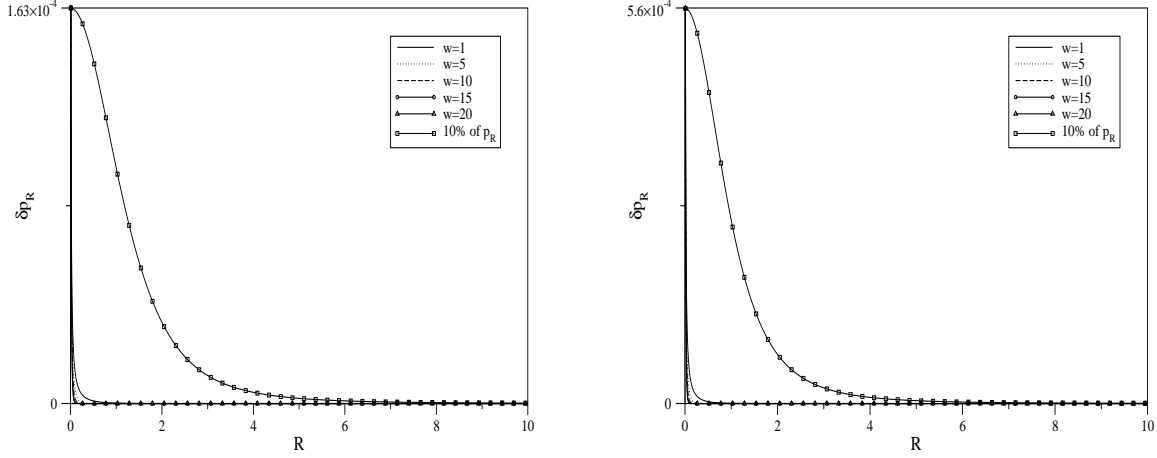


Figure 3. Profiles of the amplitude perturbation for the radial pressure of the fluid for the cases when $z = 0$ and $w = 1, 5, 10, 15, 20$. The graphs at the left and right correspond to the cases when $(a = 1, b = 1)$ and $(a = 1, b = 0.5)$ respectively. The 10% p_R profile is depicted for better stability comparisons. These modes are highly stable.

4.3 Perturbation with δU^R , δp_R , $\delta \rho$

In this subsection we perturb the radial component of the four velocity, the radial pressure and the energy density of the fluid. The set of equations (5)-(8) reduces to a second order ordinary differential equation for the perturbation δp_R of the form (20). The forms of the functions (F_A, F_B, F_C) are given in Appendix C. In this case, the coordinate z only enters as a parameter. Due to the fact that we are not considering perturbations in the azimuthal axis, the coefficients of the second order ordinary differential equation do not depend on the wavenumber k_θ . This second order equation is solved numerically with the same boundary conditions described in Sec. 4.1.

In Fig. 3 we present the amplitude profiles for different perturbation modes of the radial pressure in the plane $z = 0$ for different values of the parameters a and b . We see in the graph that the perturbation profiles decrease rapidly in few units of R . Also, the values of the radial velocity perturbation and energy density perturbation, not depicted, are well below the escape velocity and the 10% energy profile, respectively.

We performed the above analysis for different values of $-5 < z < 5$ and we found that the quantities involved have the same qualitative behavior. From these results, we can say that the general linear perturbation applied is highly stable and, for that reason, the perturbations do not form more complex structures.

4.4 Perturbation with δU^z , δp_z , $\delta \rho$

In this subsection we perturb the axial component of the four velocity, the axial component of the pressure and the energy density of the fluid. The set of equations (5)-(8) reduces to a second order ordinary differential equation for the perturbation δp_z of the form (21). The functions (F_A, F_B, F_C) are given in Appendix D. Note that, like in Sec. 4.2, the coordinate R only enters as a parameter. In this case, we are

not considering azimuthal perturbations and therefore the quantities involved do not depend on the parameter k_θ . The second order equation is solved following the procedure of Sec. 4.2.

In Fig. 4 we present the amplitude profiles of the axial pressure perturbation and the physical axial velocity perturbation, for $R = 0.1$ and for different values of the parameters a and b . We see that the axial pressure perturbation modes for $(a = 1, b = 1)$ are always of the some order of magnitude or lower when compared to the 10% profile. In the flatter case $(a = 1, b = 0.5)$, note that the amplitude of the mode $w = 1$ is greater in some region of the domain. This fact is reflected in the axial velocity perturbation profile where the mode $w = 1$ have a strange behavior. All of the modes, including the mode with $w = 1$, are stable because they are well below the escape velocity, which is not depicted. The modes that correspond to the energy density perturbation are all stable. For highly flat galaxies the mode $w = 1$ is not stable and may form more complex structures. For higher values of the parameter w the modes are more stable. We performed the above analysis for different values of the parameter $0 < R < 10$ and we found that the quantities involved have the same qualitative behavior.

4.5 Perturbation with δU^R , δp_R , δU^z , δp_z and $\delta p_R \equiv \delta p_z$

In this subsection we perturb the radial component of the four velocity, the axial component of the four velocity, the radial pressure and the axial pressure. As we said in Sec. 2, we need an extra condition to set the number of unknowns equal to the number of equations. In this case, we set $\delta p_R \equiv \delta p_z \equiv \delta p$. Therefore, the set of equations (5)-(8) reduces to a second order partial differential equation for the pressure perturbation δp , say

$$F_A \delta p_{,RR} + F_B \delta p_{,R} + F_C \delta p_{,zz} + F_D \delta p_{,z} + F_E \delta p = 0, \quad (22)$$

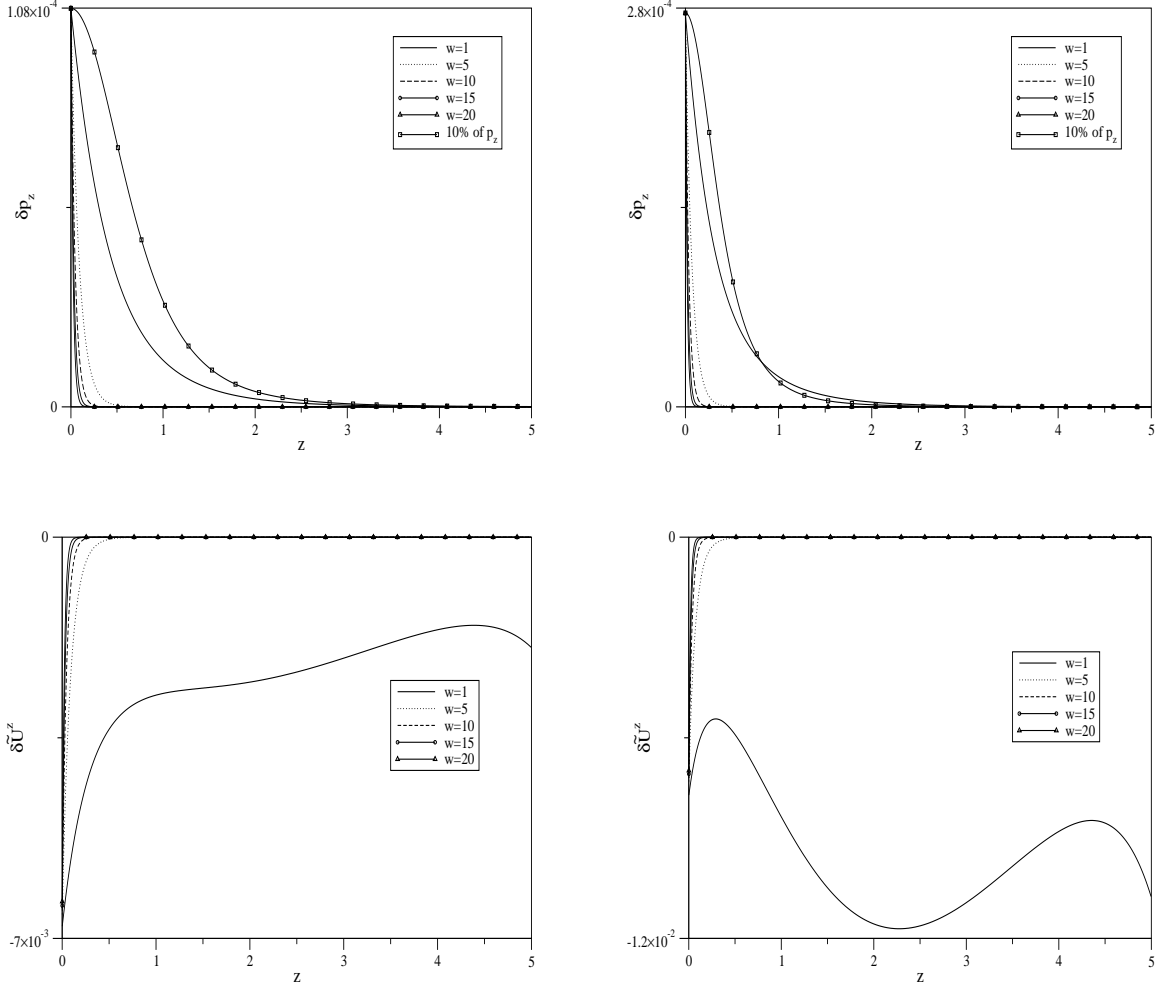


Figure 4. Profiles of the amplitude perturbation for the axial pressure and the axial physical velocity for the case when $R = 0.1$ and $w = 1, 5, 10, 15, 20$. The graphs at the left and right correspond to the cases when $(a = 1, b = 1)$ and $(a = 1, b = 0.5)$ respectively. The 10% p_z profile is depicted in the graph of δp_z for better stability comparisons. In the graph of $\delta \tilde{U}^z$ the escape velocity is not depicted because it is several orders of magnitude greater. For these examples all the modes are stable, but for a highly flat galaxy some modes, like the mode with $w = 1$, are not stable.

where $(F_A, F_B, F_C, F_D, F_E)$ are functions of (R, z, w) , see Appendix E. The partial differential equation (22) is solved numerically with four boundary conditions, at $z = -Z_{cut}$, $z = Z_{cut}$, $R \approx 0$ and $R = R_{cut}$. They are different ways in which we can set the boundary conditions in order to simulate various kinds of pressure perturbations. Here, we treat only the case when we have a pressure perturbation at $R \approx 0$ and along the z axis, i.e. some kind of a rod perturbation. We set the value of the rod pressure perturbation to be 10% of the axial pressure. We set the values of the other boundary conditions equal to zero because we want the perturbation to vanish when approaching the edge of the disk. We choose the 10% of the value of the axial pressure instead of the radial pressure because it has the lowest value near $R \approx 0$. In that way, the perturbation values are also below the 10% values of the radial pressure and the general linear perturbation is valid.

In Fig. 5, we present the perturbation amplitudes for the pressure, the physical radial velocity and the physical axial velocity, for $w = 1$ and for different values of the parameters a and b . We see in the pressure perturbation graph that the perturbation rapidly decays to values near zero when we move out from the center of the disk. This behavior is the same for every galaxy considered. In the velocity perturbations profiles we can see a phenomenon that is more clear in the flatter galaxy. Note that in the lower domain of the disk $[-5, 0)$ the axial velocity perturbation is positive and in the upper domain $(0, 5]$ the axial velocity perturbation is negative. This means that due to the linear perturbation the disk tries to collapse to the plane $z = 0$. Now, if we look to the radial velocity perturbation graph, we note that the upper and lower parts depart from the center of the disk due to the positive radial perturbation. So, with these considerations, we may say that the disk tends to form some kind of ring

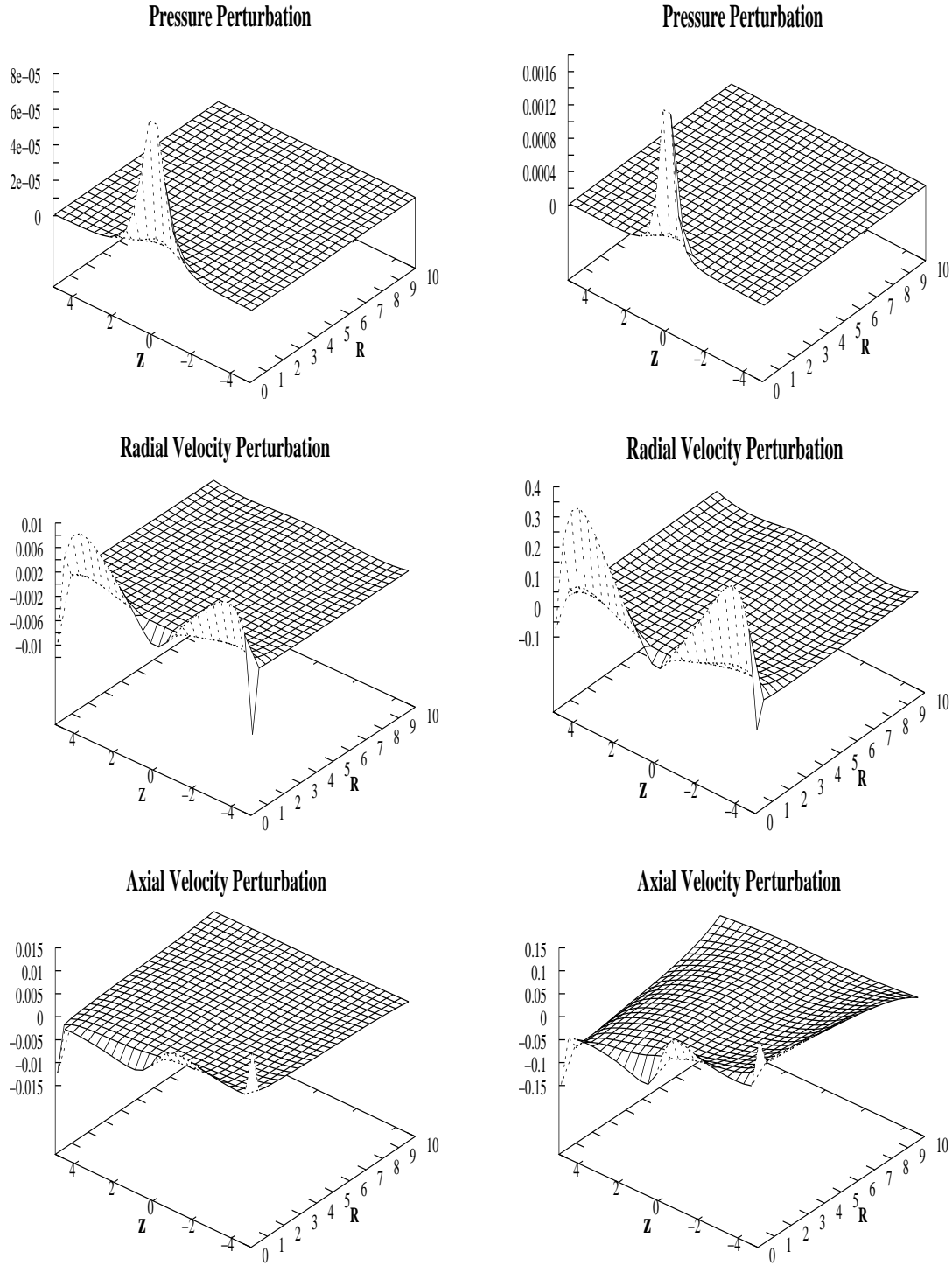


Figure 5. Profiles of the amplitude perturbation for the pressure, the radial physical velocity and the axial physical velocity of the fluid for the case when $w = 1$ and for a rod perturbation in $R \approx 0$. With this kind of perturbation the disk tends to form some kind of ring around the center of the disk. This phenomenon is greater for highly flat galaxies and lower for more spherical systems.

around the center of the disk. This phenomenon is greater for highly flat galaxies and lower for more spherical systems.

5 CONCLUSIONS

In this article we studied the stability of the recently proposed general relativistic Miyamoto-Nagai model [Vogt & Letelier (2005b)] by applying a general first order perturbation. We can say that the stability analysis performed is more complete than the stability analysis of particle motion along geodesics because we have taken into account the collective behavior of the particles. However, this analysis can be said to be incomplete because the energy momentum perturbation tensor of the fluid is treated as a test fluid and does not alter the background metric. This is a second degree of approximation to the stability problem in which the emission of gravitational radiation is considered.

The different stability analyses made to the general relativistic Miyamoto-Nagai disk show that this disk is stable for higher values of the wave number k_θ and the frequency w . For lower values of k_θ and w the disk presents not-stable modes that may form more complex structures like rings, bars or halos, but in order to study them we need a higher order perturbation formalism. In general, not-stable modes appear more for flatter galaxies and less for spherical systems.

ACKNOWLEDGMENTS

M.U. and P.S.L. thanks FAPESP for financial support; P.S.L. also thanks CNPq.

APPENDIX A: FUNCTIONS F_A , F_B AND F_C OF SECTION 4.1

The general form of the functions (F_A, F_B, F_C) appearing in the second order ordinary differential equation (20) is given by

$$\begin{aligned} F_A &= A_1\alpha_1, & F_B &= A_1\alpha_{1,R} + A_1\alpha_2 + A_3\alpha_1, \\ F_C &= A_1\alpha_{2,R} + A_3\alpha_2 + A_4\alpha_3, \end{aligned} \quad (A1)$$

where α_1 , α_2 and α_3 are

$$\begin{aligned} \alpha_1 &= -\frac{B_1}{B_2}, & \alpha_2 &= \frac{B_5D_4 - B_4D_5}{B_2D_5}, \\ \alpha_3 &= \frac{C_2D_4}{C_1D_5}. \end{aligned} \quad (A2)$$

In Eqs. (A1) and (A2), we denote the coefficients of Eq. (5) by A_i , the coefficient of Eq. (6) by B_i , the coefficient of Eq. (7) by C_i , the coefficient of Eq. (8) by D_i , e.g., the first term in (5) has the coefficient A_1 multiplied by the factor $\delta U_{,R}^R$, the second term has the coefficient A_2 multiplied by the factor δU^R , etc. The explicit form of the above equations is obtained replacing the fluid variables (ρ, p_R, p_θ, p_z) of the isotropic Schwarzschild thick disk.

APPENDIX B: FUNCTIONS F_A , F_B AND F_C OF SECTION 4.2

The general form of the functions (F_A, F_B, F_C) appearing in the second order ordinary differential equation (21) is given by

$$\begin{aligned} F_A &= A_2\alpha_1, & F_B &= A_2\alpha_{1,z} + A_2\alpha_2 + A_5\alpha_1, \\ F_C &= A_2\alpha_{2,z} + A_4\alpha_3 + A_5\alpha_2, \end{aligned} \quad (B1)$$

where α_1 , α_2 and α_3 are

$$\begin{aligned} \alpha_1 &= -\frac{D_1}{D_2}, & \alpha_2 &= \frac{B_6D_5 - B_5D_6}{B_5D_2}, \\ \alpha_3 &= \frac{C_2B_6}{C_1B_5}, \end{aligned} \quad (B2)$$

and the meaning of the coefficients (A_i, B_i, C_i, D_i) is explained in Appendix A.

APPENDIX C: FUNCTIONS F_A , F_B AND F_C OF SECTION 4.3

The general form of the functions (F_A, F_B, F_C) is given by

$$\begin{aligned} F_A &= A_1\alpha_1, & F_B &= A_1\alpha_{1,R} + A_1\alpha_2 + A_3\alpha_1, \\ F_C &= A_1\alpha_{2,R} + A_3\alpha_2 + A_6\alpha_3, \end{aligned} \quad (C1)$$

where α_1 , α_2 and α_3 are

$$\begin{aligned} \alpha_1 &= -\frac{B_1}{B_2}, & \alpha_2 &= \frac{B_3D_4 - B_4D_3}{B_2D_3}, \\ \alpha_3 &= -\frac{D_4}{D_3}, \end{aligned} \quad (C2)$$

and the meaning of the coefficients (A_i, B_i, D_i) is explained in Appendix A.

APPENDIX D: FUNCTIONS F_A , F_B AND F_C OF SECTION 4.4

The general form of the functions (F_A, F_B, F_C) is given by

$$\begin{aligned} F_A &= A_2\alpha_1, & F_B &= A_2\alpha_{1,z} + A_2\alpha_2 + A_5\alpha_1, \\ F_C &= A_2\alpha_{2,z} + A_5\alpha_2 + A_6\alpha_3, \end{aligned} \quad (D1)$$

where α_1 , α_2 and α_3 are

$$\begin{aligned} \alpha_1 &= -\frac{D_1}{D_2}, & \alpha_2 &= \frac{B_6D_3 - B_3D_6}{B_3D_2}, \\ \alpha_3 &= -\frac{B_6}{B_3}, \end{aligned} \quad (D2)$$

and the meaning of the coefficients (A_i, B_i, D_i) is explained in Appendix A.

APPENDIX E: FUNCTIONS F_A, F_B, F_C, F_D AND F_E OF SECTION 4.5

The general form of the functions (F_A, F_B, F_C, F_D, F_E) appearing in the partial second order differential equation (22) is given by

$$\begin{aligned} F_A &= A_1\alpha_1, & F_B &= A_1\alpha_{1,R} + A_1\alpha_2 + A_3\alpha_1, \\ F_C &= A_2\alpha_3, & F_D &= A_2\alpha_{3,z} + A_2\alpha_4 + A_5\alpha_3, \\ F_E &= A_1\alpha_{2,R} + A_2\alpha_{4,z} + A_3\alpha_2 + A_5\alpha_4, \end{aligned} \quad (\text{E1})$$

where $\alpha_1, \alpha_2, \alpha_3$ and α_4 are

$$\begin{aligned} \alpha_1 &= -\frac{B_1}{B_2}, & \alpha_2 &= -\frac{B_4 + B_6}{B_2}, \\ \alpha_3 &= -\frac{D_1}{D_2}, & \alpha_4 &= -\frac{D_4 + D_6}{D_2}. \end{aligned} \quad (\text{E2})$$

and the meaning of the coefficients (A_i, B_i, D_i) is explained in Appendix A.

REFERENCES

- Abramowicz M.A., Prasanna A.R., MNRAS, 245, 720
 Bardeen J.M., 1970, ApJ, 161, 103
 Bičák J., Ledvinka T., 1993, Phys. Rev. Lett., 71, 1669
 Bičák J., Lynden-Bell D., Katz J., 1993, Phys. Rev. D, 47, 4334
 Bičák J., Lynden-Bell D., Pichon C., 1993, MNRAS, 265, 126
 Binney J., Tremaine S., 1987, Galactic Dynamics, Princeton University Press, New Jersey
 Bonnor W.B., Sackfield A., 1968, Commun. Math. Phys., 8, 338
 Chazy J., 1924, Bull. Soc. Math. France, 52, 17
 Curzon H.E.J., 1924, Proc. London Math. Soc., 23, 477
 Frauendiener J., Klein C., 2001, Phys. Rev. D, 63, 084025
 Fridman A.M., Polyachenko V.L., 1984, Physics of Gravitating Systems I : Equilibrium and Stability, Springer-Verlag, New York
 García-Reyes G., González G.A., 2004, Phys. Rev. D, 69, 124002
 González G.A., Espitia O.A., 2003, Phys. Rev. D, 68, 104028
 González G.A., Letelier P.S., 1999, Class. Quantum Grav., 16, 479
 González G.A., Letelier P.S., 2000, Phys. Rev. D, 62, 064025
 González G.A., Letelier P.S., 2004, Phys. Rev. D, 69, 044013
 Kalnajs A.J., 1972, ApJ, 175, 63
 Karas V., Huré J.-M., Semerák O., 2004, Class. Quantum Grav., 21, R1
 Katz J., Bičák J., Lynden-Bell D., 1999, Class. Quantum Grav. 16, 4023
 King I.R., 1966, Astron. J., 71, 64
 Klein C., 1997, Class. Quantum Grav., 14, 2267
 Klein C., 2001, Phys. Rev. D, 63, 064033
 Klein C., 2002, Phys. Rev. D, 65, 084029
 Klein C., 2003a, Phys. Rev. D, 68, 027501
 Klein C., 2003b, Ann. Phys. (N.Y.), 12, 599
 Klein C., Richter O., 1999, Phys. Rev. Lett., 83, 2884
 Kuzmin G.G., 1956, Astron. Zh., 33, 27
 Landau L.D., Lifshitz E.M., 1987, Fluid Mechanics, 2nd ed., Pergamon Press, Oxford, Sec. 27
 Ledvinka T., Zofka M., Bičák J., 1999, Proceedings of the 8th Marcel Grossman Meeting in General Relativity, edited by T. Piran, World Scientific, Singapore, 339
 Lemos J.P.S., 1989, Class. Quantum Grav., 6, 1219
 Lemos J.P.S., Letelier P.S., 1993, Class. Quantum Grav., 10, L75
 Lemos J.P.S., Letelier P.S., 1994, Phys. Rev. D, 49, 5135
 Lemos J.P.S., Letelier P.S., 1996, Int. J. Mod. Phys. D, 5, 53
 Letelier P.S., 1999, Phys. Rev. D, 60, 104042
 Letelier P.S., 2003, Phys. Rev. D, 68, 104002
 Lord Rayleigh, 1916, Proc. R. Soc. London, A93, 148
 Lynden-Bell D., Pineault S., 1978, MNRAS, 185, 679
 Mestel L., 1963, MNRAS, 126, 553
 Miyamoto M., Nagai R., 1975, PASJ, 27, 533
 Morgan L., Morgan T., 1970, Phys. Rev. D, 2, 2756
 Morgan T., Morgan L., 1969, Phys. Rev., 183, 1097
 Nagai R., Miyamoto M., 1976, PASJ, 28, 1
 Neugebauer G., Meinel R., 1995, Phys. Rev. Lett., 75, 3046
 Plummer H.C., 1911, MNRAS, 71, 460
 Satoh G., 1980, PASJ, 32, 41
 Seguin F.H., 1975, ApJ, 197, 745
 Semerák O., 2002, Gravitation: Following the Prague Inspiration, to Celebrate the 60th Birthday of Jiri Bičák, edited by Semerák O., Podolsky J., Zofka M., World Scientific, Singapore, 111, available at <http://xxx.lanl.gov/abs/gr-qc/0204025>.
 Semerák O., 2003, Class. Quantum Grav., 20, 1613
 Semerák O., Žáček M., 2000a, PASJ, 52, 1067
 Semerák O., Žáček M., 2000b, Class. Quantum Grav., 17, 1613
 Toomre A., 1963, ApJ, 138, 385
 Ujevic M., Letelier P.S., 2004, Phys. Rev. D, 70, 084015
 Ujevic M., Letelier P.S., 2005, A&A, 442, 785
 Ujevic M., Letelier P.S., 2006, J. Comput. Phys., 215, 485
 Ujevic M., Letelier P.S., 2007, Gen. Relativ. Gravit., DOI: 10.1007/s10714-007-0438-y
 Vogt D., Letelier P.S., 2003, Phys. Rev. D, 68, 084010
 Vogt D., Letelier P.S., 2004a, Class. Quantum Grav., 21, 3369
 Vogt D., Letelier P.S., 2004b, Phys. Rev. D, 70, 064003
 Vogt D., Letelier P.S., 2005a, Phys. Rev. D, 71, 084030
 Vogt D., Letelier P.S., 2005b, MNRAS, 363, 268
 Vogt D., Letelier P.S., 2007, Triaxial Analytical Potential-Density Pair for Galaxies, PAJS, in press
 Voorhees B.H., 1970, Phys. Rev. D, 2, 2119
 Zipoy D.M., 1966, J. Math. Phys., 7, 1137